WARSAW UNIVERSITY OF TECHNOLOGY Index 351733
FACULTY OF CIVIL ENGINEERING
COMMITTEE FOR CIVIL AND WATER ENGINEERING
POLISH ACADEMY OF SCIENCES ISSN 1230-2945
DOI: 10.24425/ace.2026.158614
ARCHIVES OF CIVIL ENGINEERING
Vol. LXXII ISSUE 2 2026
pp. 363–376

Research paper

Safety management method for foundation pit design of a subway station: based on stability analysis and deformation monitoring of the foundation pit

Liping Zhao[1]

Abstract: In order to effectively monitor the stability data of foundation pit during the construction process, the study proposes a monitoring model that can monitor the deformation state of foundation pit in subway stations in real time. The study analyzes the force state of the support through the deformation mode and extrusion direction of the soil layer, and calculates the displacement and deformation of the soil layer by combining with the hydrological environment around the soil layer. Data monitoring points are set up to monitor the dynamic data of key stress areas. The study was conducted to predict the deformation state of foundation pit with long short-term memory artificial neural network model, combined with fast Lagrangian analysis of continuum for numerical validation. The study revealed that the accuracy of prediction of test data with the research monitoring model was 0.912. The convergence speed of the research model during training was 37.34–38.27% higher than other methods. Meanwhile, the data occupancy of the research model in the prediction process was low and its redundancy was reduced by 10.74–36.17% compared to other methods. During the data prediction process of foundation pit, the mean accuracy of the research method for the prediction of wall deformation and settlement of foundation pit remained above 95%. Therefore, the research method provides an efficient monitoring model for the safety management of foundation pit design in subway stations.

Keywords: displacement deformation, long short-term memory, pit construction, subway construction

[1]PhD., Eng., Anyang Vocational and Technical College, School of Architectural Design and Engineering, Anyang 455000, China, e-mail: zlp202405@163.com, ORCID: 0009-0009-7768-6972

1. Introduction

With the modernization and development of the city, the subway lines of urban transportation are becoming increasingly complex, and the environmental factors that need to be considered in the subsequent subway construction are also more and more [1]. At present, the spatial scope of subway construction involves more areas, and the construction process of FP design safety management methods are not enough to analyze the mechanical state changes in the construction process [2]. Earlier studies uses the total stress method to calculate the soil layer (SL) pressure as well as the shear state during excavation. These studies analyzes the mechanical state based on the overall structure of the SL, and judges the deformation state of the SL by combining the pore ratio and other parameters [3]. The surface settlement calculation method, on the other hand, judges the subsidence caused by deformation on the basis of stress analysis. This approach effectively predict the surface deformation of FP by calculating the surface settlement value of FP with exponential curve fitting method with the help of SL composition analysis [4]. However, monitoring the state change of FP SL only by theoretical calculation method cannot get the mechanical state change of FP in time. With the updating of numerical analysis methods, fast Lagrangian analysis of continuum (FLAC) method is used for simulation prediction of FP engineering. However, the simulation process of this method is limited by the monitoring distribution and parameter setting [5].

To monitor the soil deformation data during the construction of subway foundation pit (FP), researchers have conducted a series of studies on FP deformation monitoring methods. Dong Y et al. suggested a detection method based on time function model for FP monitoring during subway facilities. The outcomes showed that the suggested approach could successfully keep an eye on the surrounding pile body's support stability [6]. A clustering monitoring approach based on a Gaussian mixture model was put up by Zhang et al. to address the issue of soil settlement on both sides of the subway FP. The research results indicated that the proposed method had faster data classification effect for the monitoring of FP data [7]. For FP monitoring in seasonal permafrost regions, Wang et al. suggested a method based on spatial effect and deformation prediction. Based on the study's findings, the suggested approach might be able to effectively monitor FP construction in seasonal permafrost layers [8]. Liu et al. suggested a method based on soil creep monitoring for FP monitoring in muddy clay layers. The outcomes showed that the suggested approach could successfully track FP's condition of deformation in a muddy clay layer [9]. For the deformation of the formation during FP excavation, Feng et al. developed a study model based on the back propagation (BP) network algorithm and the artificial bee colony algorithm. According to the study's findings, the suggested strategy could accurately forecast how the ground will shift during FP construction [10].

Sun proposed a research method based on FLAC for the problem of municipal landfill. The study was conducted to simulate the zoning of SLs through the investigation of soil parameters. The outcomes demonstrated the efficacy of the suggested approach in forecasting the status of soil alterations in landfills [11]. Song et al. suggested a method based on the study of FLAC 3D simulation for the hydraulic impact problem of coal bed floor. The study's findings suggested that the suggested strategy might successfully stop water flow from having an undue influence on the coal seam base plate [12]. Jing et al. proposed a triaxial test method based on FLAC for

the problem of analyzing the force effect of soybean materials. The study's findings suggested that the suggested technique could examine the material's and the stressing surface's mechanical state with effectiveness [13]. Zhang et al. suggested a technique for the force analysis of coarse-grained soil material that combined FLAC with a particle flow code. The findings showed that the suggested approach could efficiently assess and track coarse-grained soil's filling and deformation processes [14]. Miao et al. proposed a recursive neural network algorithm based on long short-term memory (LSTM) for the deterioration of concrete bridges. The study's findings suggested that the strategy could accurately identify bridge deterioration regions [15].

In summary, the current research on the construction monitoring of subway FP is dominated by the numerical analysis method. However, this method relies on the setting of model parameters, and the monitoring of data is relatively decentralized. In addition, due to the difficulty in predicting and accurately assessing various complex factors during excavation construction, it may cause instability of supporting structures, damage to the surrounding environment, or hydrogeological disasters. For example, if a slip surface is formed in the soil, the retaining structure, along with the soil outside and at the bottom of the FP, will lose stability. There is significant settlement or severe cracking of the surrounding ground. Therefore, the study innovatively combines the LSTM method with the FLAC method, and collects early FP deformation data to train the LSTM model. In order to provide an efficient technological solution for the stability investigation of FP in subway stations, the model's prediction results are utilized to filter the parameters and monitoring points of FLAC simulation.

2. Methods and materials

2.1. Support and stability of FP in subway station

Although underground transportation eases traffic congestion on the roads to a great extent, geological factors can also have an impact on the building of this type of transportation, increasing the risk of accidents both during and after construction [16, 17]. Therefore, the deformation trend of FP and the supporting structure need to be analysed initially. The direction of the earth pressure (EP) causes the position of the wall to be offset to one side. The types of soil pressure are mainly divided into three categories, the rest of pressure tends to have no displacement bias on the wall, while both active and passive types of soil pressure cause the position of the wall to be offset. The active type of EP is used to calculate the value of pressure caused by active type of EP using Rankine EP theory as shown in Eq. (2.1).

$$\begin{cases} E_a = [K_a \gamma (H - z_0)^2] / 2 \\ z_0 = (2c) / (\gamma \sqrt{K_a}) \end{cases} \tag{2.1}$$

In Eq. (2.1), E_a denotes the total EP value of the active type. K_a is the EP coefficient of the active type. γ is the value of the SL's unit weight. H is the height of the wall. z_0 denotes the depth value of the calculated locus. c denotes the cohesion of the SL. The passive EP value is expressed as shown in Eq. (2.2).

$$E_p = \frac{1}{2} \gamma H^2 K_p + 2cH\sqrt{K_p} \tag{2.2}$$

In Eq. (2.2), E_p denotes the passive total EP value. K_p denotes the passive EP coefficient under the current soil property. For the problem of arching on FP, it can be calculated by the method of factor of safety against arching as shown in Eq. (2.3).

$$\frac{cN_c + \gamma' t N_q}{(\gamma h_1 + \gamma_{\text{sat}} h_2 + \gamma' t) + q} \geq K_h \tag{2.3}$$

In Eq. (2.3), N_c denotes the bearing capacity (BC) coefficient of the SL. γ' denotes submerged unit weight of the SL. t denotes the distance between groundwater and the underlying wall. N_q denotes the BC coefficient of foundation soil in the near groundwater layer. h_1 denotes the thickness of the upper SL of the outer groundwater layer. γ_{sat} denotes the saturated gravity value of the SL. h_2 denotes the thickness of the SL between the inner and outer layers. q denotes the applied force of the upper layer. K_h denotes the factor of safety against arching. When the upward arching trend is formed, the deformation state of FP enclosure will be as shown in Fig. 1.

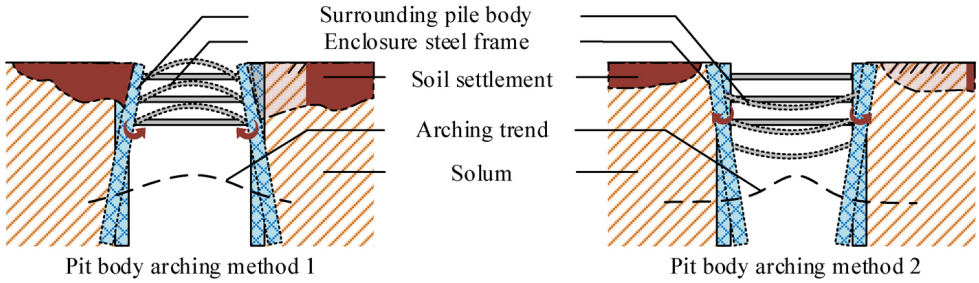

Fig. 1. Displacement and deformation mode of FP

In Fig. 1, when the subsoil uplift occurs, the enclosure on both sides will have either an upper inward tilt or a lower inward tilt. The inward tilt of the upper layer is due to the low analysis result of the load force of the upper layer in the calculation, while the inward tilt of the lower layer is due to the deformation of the substructure caused by the passive force. The SL of FP will settle and deform after excavation of FP because of the limited resistance of the support. The subsidence patterns of the ground surface are mainly categorized into depressed and triangular forms. The concave form of surface subsidence exerts high pressure on the middle SL of the enclosure, resulting in deformation of the middle part of the support. The triangular form of surface subsidence exerts greater pressure on both the middle and upper SLs of the enclosure, resulting in deformation of both the middle and upper parts of the support. The influence range caused by simultaneous subsidence is shown in Eq. (2.4).

$$x_0 = H_g \tan\left(45^\circ - \frac{\varphi}{2}\right) \tag{2.4}$$

In Eq. (2.4), H_g denotes the height value of the enclosure. φ indicates the average value of internal friction angle between the enclosure and the SL. According to the degree of subsidence and the range of subsidence waves on the support form of the enclosure and support materials to make corresponding adjustments, to ensure that the enclosure on the effective support of the SL.

2.2. Construction of deformation monitoring model for FP in subway station

The deformation law and displacement parameters of the subway FP excavation can be established by analyzing the deformation effect between the enclosure and the SL. However, using the change rule of mechanics alone to analyze every deformation condition during the subway construction process is extremely challenging [18, 19]. Moreover, the effect of deformation of FP due to soil property and hydrological environment in the soil environment is difficult to be calculated in a single way [20]. Thus, by using the LSTM approach, the study predicts the deformation of FP in the construction area and visualizes the force state of FP through 3D simulation. Mechanical simulation of the deep pit construction method is carried out with the help of FLAC numerical checking method to realize the effective monitoring of FP deformation. The monitoring setup is carried out by laying the inclined pipe near the piles in different construction sections. The course of action of the skew tube is shown in Fig. 2.

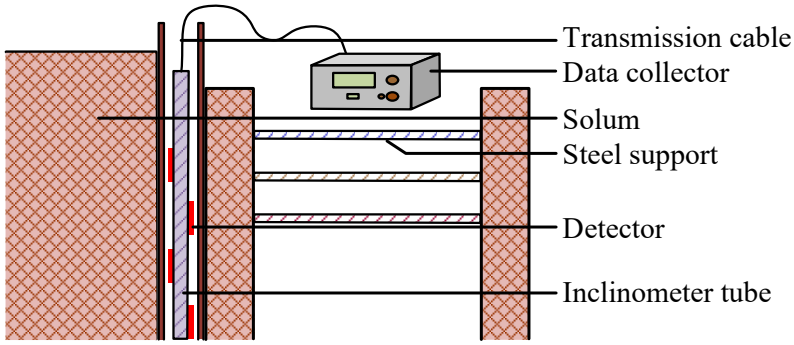

Fig. 2. The working principle of inclinometer tube

In Fig. 2, the inclinometer tube is embedded vertically into the FP soil, and a data detector is placed inside the inclinometer tube, which is connected to an external data collector by a transmission cable. Equation (2.5) illustrates how the shear modulus of the SL can be simultaneously determined for various soil property based on the displacement of the soil.

$$G_0 = G_0^{\text{ref}} \left(\frac{c \cos \varphi + \sigma_3 \sin \varphi}{c \cos \varphi + p^{\text{ref}} \sin \varphi} \right)^m \tag{2.5}$$

In Eq. (2.5), G_0 denotes the shear initial modulus. σ_3 denotes the shear modulus coefficient. G_0^{ref} denotes the shear initial modulus when the pressure is p^{ref}. m denotes the exponential power value of the setting. The dynamic shear strain relationship can be obtained by combining the strain force calculation of SLs. This study adopts the strain model proposed by Santos and Correia, as shown in Eq. (2.6).

$$\frac{G}{G_0} = \frac{1}{1 + a \left| \frac{\gamma}{\gamma_r} \right|} \tag{2.6}$$

In Eq. (2.6), G denotes the shear modulus. a denotes the shear strain coefficient. γ denotes the current shear strain. γ_r denotes the reference shear strain. The value of shear strain force can be calculated by the soil strain law expansion form as shown in Eq. (2.7).

$$\gamma = \sqrt{3}\frac{\|H'\Delta e'\|}{\|\Delta e'\|} \tag{2.7}$$

In Eq. (2.7), H' denotes the past symmetric tensor of the applied material. $\Delta e'$ denotes the actual bias strain increment. Two mechanical curves can be obtained when both axial strain and bias stress of the soil model are applied. According to the relationship between the two curves the stress expression can be obtained as shown in Eq. (2.8).

$$\begin{cases} \varepsilon_1 = \dfrac{1}{E_i}\dfrac{q}{1-q/q_a}, & q < q_f \\ E_i = \dfrac{2E_{50}}{2-R_f} \end{cases} \tag{2.8}$$

In Eq. (2.8), ε_1 denotes the axial strain. E_i denotes the initial value of elastic modulus. q denotes the bias stress. q_f denotes the limiting value of the bias stress. q_a denotes the value of strength change in shear. E_{50} denotes the cut line modulus at half ultimate load. R_f denotes the breaking ratio. To analyze and monitor the overall construction status of the subway FP, the structural section of the subway FP is drawn as shown in Fig. 3.

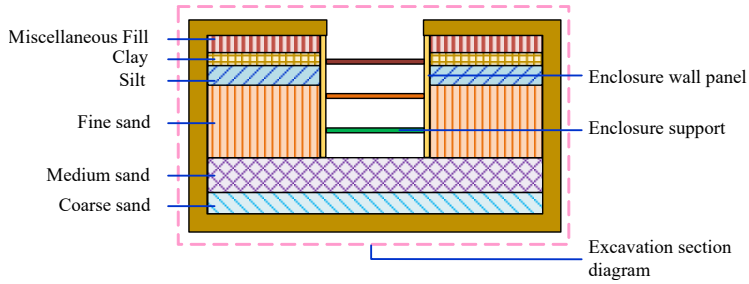

Fig. 3. Structural sectional drawing of subway FP

In Fig. 3, the FP subway station adopts a composite support system. The concave FP located in the middle of the SL is supported by enclosure. In the enclosure process, the vertical rigid support is provided by the grouted piles, and the horizontal support is provided by the steel support (SS). The SS is added gradually according to the layering. The moment of inertia of the steel structure is expressed as shown in Eq. (2.9).

$$I = \frac{1}{32}\pi(R^4 - r^4) \tag{2.9}$$

In Eq. (2.9), I denotes the transverse moment of inertia of the steel pipe. R and r are the outer and inner radius of the steel pipe. Enclosure structure and FP structure are simulated by FLAC software for the working condition of subway construction. The parameters of concrete materials for different soil types are shown in Table 1.

Table 1. Concrete material parameters

Soil type	Elastic modulus (MPa)	Poisson's ratio	Compressive strength (MPa)
Miscellaneous fill	35	0.38	0.8
Clay	25	0.40	0.5
Silt	60	0.35	1.2
Fine sand	80	0.30	2.0
Medium sand	120	0.28	3.5
Coarse sand	180	0.25	5.0

This study uses the Mohr–Coulomb constitutive model in FLAC software to simulate the F. The mechanical boundary conditions are the lateral constraint normal displacement of the model and the horizontal and vertical constraint displacements at the bottom of the model. The water head boundary condition is that the bottom of the model is an impermeable boundary, and the four side boundaries of the model are constant water head boundary conditions. The FP's radial displacement and structural deformation are predicted using the LSTM model, which helps to further monitor the FP's construction state. The study adopts the mean squared error (MSE) loss function as the optimization objective function of the LSTM model, as shown in Eq. (2.10).

$$L = \frac{1}{N}\sum_{i=1}^{N}(y - y_i) \tag{2.10}$$

In Eq. (2.10), y represents the true value and y_i represents the predicted value. When the prediction error exceeds the set threshold, the LSTM performs BP to correct the hyperparameters based on the obtained loss function value. In this study, tenfold cross-validation is used to train the LSTM model, and the algorithm is optimized using Adam. After network training, the data model can predict the displacement and settlement changes of the FP. The workflow of subway foundation pit deformation monitoring is shown in Fig. 4.

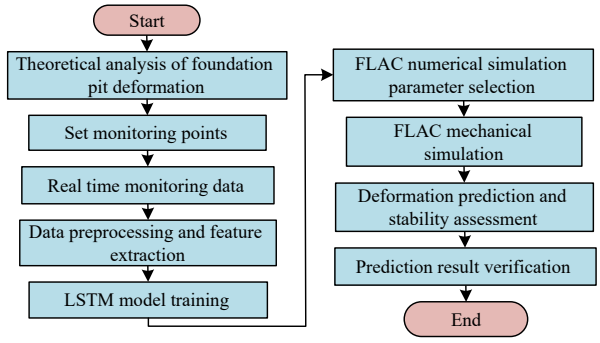

Fig. 4. Monitoring process for deformation of subway FP

Figure 4 shows how the deformation theory of FP is used to examine FP design safety management before calculating the deformation of FP's internal enclosure structure and the surrounding environment. Combine with FLAC software to model the FP data. The construction monitoring is carried out according to the numerical calculation results, and the advancement of the project is determined by the LSTM-FLAC model.

3. Results

3.1. Performance testing of FP monitoring models for subway stations

The study uses Adam optimizer and L2 regularization, with batch size set to 32, learning rate set to 0.001, and number of hidden layer units set to 64. The data information of 12 monitoring points is selected as the training dataset. The iterations of the model is set to 250 times. For testing, 3 random monitoring point data are selected as the test dataset. The BP algorithm can automatically learn and model complex nonlinear relationships, and comprehensively consider the influence of multiple factors on FP deformation [21]. ARIMA algorithm can effectively capture trends, seasonality, and periodicity in the data, and is suitable for data analysis with time series characteristics, such as subway FP deformation monitoring [22]. BP algorithm and ARIMA algorithm are used as comparative algorithms. The comparison of the iterative effects of the three methods is shown in Fig. 5.

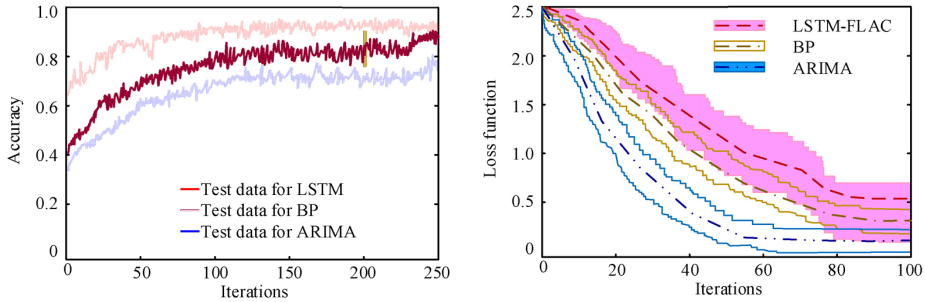

Fig. 5. Comparison of model performance: (a) Accuracy, (b) Fitness

In Fig. 5(a), the accuracy of the LSTM-FLAC model for the dataset test of FP improves with the increase of the number of iterations. And the accuracy curve of the study model is higher than the BP algorithm and ARIMA algorithm. The final prediction accuracy (PA) of LSTM-FLAC algorithm tested after 250 iterations reaches 0.912. The final PA of BP algorithm reaches 0.884. The final PA of ARIMA algorithm reaches 0.781. The accuracy of the research model improves by 2.8-13.1% compared to BP and ARIMA algorithms. In Fig. 5(b), the LSTM-FLAC algorithm for the dataset test loss function for the FP decreases with the increase in the iterations. The convergence speed of the research model is better than the BP algorithm and ARIMA algorithm, and the convergence speed of the objective function is 37.34-38.27% faster. It indicates that the research model is better at monitoring FP data. The CPU occupancy and running data bandwidth detection results of the model are acquired as illustrated in Fig. 6 for additional testing of the model's operating performance.

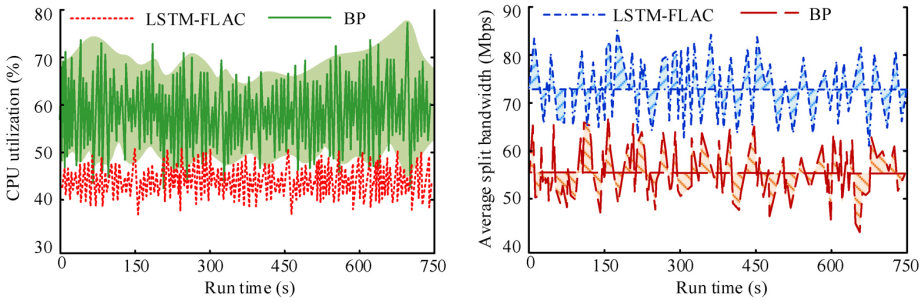

(a) (b)

Fig. 6. Efficiency testing of model operation: (a) CPU utilization, (b) Average split bandwidth

In Fig. 6(a), when the prediction commands are executed with the BP model, the CPU occupancy of the machine ranges from 43.91-77.29%, and the average CPU occupancy is 61.34%. When the LSTM-FLAC model executes the prediction commands, the CPU occupancy of the machine ranges from 33.17-54.22%. Compared to the BP model, the CPU occupancy of the LSTM-FLAC model is reduced by 10.74-36.17%. In Fig. 6(b), the average segmentation bandwidth performance of the machine is 62.17-85.26 Mbps when the prediction of 50 FP data is performed simultaneously with LSTM-FLAC model. The average segmentation bandwidth performance of the machine is 44.74Mbps-67.28Mbps when the prediction of 50 FP data is performed simultaneously with BP model. The average segmentation bandwidth mean performance is 55.06 Mbps. Compared to the BP model, the average segmentation bandwidth of the LSTM-FLAC model is 17.43-45.23% higher. It suggests that the research method's model prediction performance is superior. The actual machine operation is better in performing FP data prediction. The process runs less occupied and the model's prediction process is smoother. Prediction is carried out in LSTM- FLAC and BP models with 250 test samples in order to further evaluate the predictive power of the model. The prediction anomaly results are shown in Fig. 7.

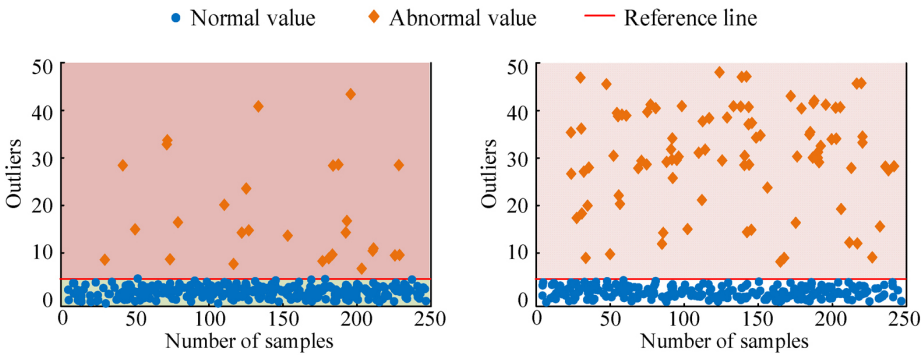

(a) (b)

Fig. 7. Comparison of model prediction outliers: (a) LSTM-FLAC, (b) BP

In Fig. 7(a), the LSTM-FLAC model is used to test the FP data samples and compare the results between the prediction results and monitoring results for anomaly assessment. It can be noticed that most of the samples are concentrated below the reference line when the research algorithm performs data prediction. The anomaly deviation between the prediction results and the monitoring results is relatively low, and the final anomaly rate of the overall samples in the LSTM-FLAC model shows 6.23%. In Fig. 7(b), the prediction of FP data with BP model yields a large anomaly deviation between the predicted and monitored values. The anomalous sample data on the reference line increases, and the final performance of the overall sample data anomaly rate is obtained as 18.63%, which is 12.4% higher compared to the LSTM-FLAC method. It shows that in the actual prediction process, the LSTM-FLAC model has better data prediction results for the subway FP, and the probability of data prediction deviation is smaller. Moreover, the data predicted by the research model is more in line with the monitoring results, which is beneficial to the deformation monitoring and stability analysis during the construction process.

3.2. Testing the application effect of FP monitoring model in subway stations

Five monitoring locations at the subway FP construction are chosen for priority prediction and synchronized monitoring in order to evaluate the study method's practical application effect for FP monitoring. The monitoring unit for numerical analysis is set to be 10m. According to the data prediction of the research method, the displacement change and settlement degree of different monitoring points are obtained as shown in Fig. 8.

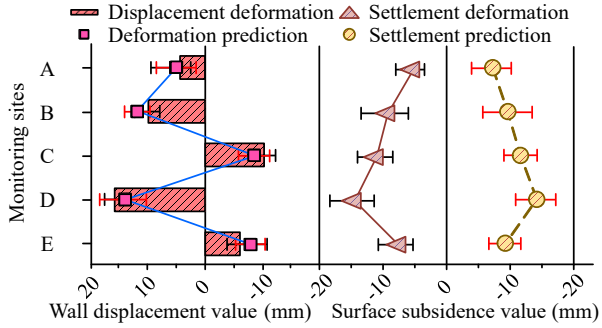

Fig. 8. Changes in displacement and settlement of FP

In Fig. 8, at monitoring point A, the difference between the settlement predicted by the study method for FP wall and the monitored value is 1.36%. For the FP wall, the difference between the predicted and monitored settlement (DPMS) values is 2.38%. At monitoring point B, the DPMS of FP wall by the study method is 3.68%. The DPMS values for the FP wall is 3.66%. At monitoring point C, the difference between the settlement predicted by the study method for FP walls and the monitored values is 2.55%. The settlement predictions for FP walls differed from the monitored values by 1.83%. At monitoring point D, the difference between the settlement predictions and the monitored values for the FP wall by the study method is 4.03%. The DPMS values for the FP wall is 6.69%. At monitoring point E, the DPMS values

of FP wall by the research method is 3.96%. The DPMS values of FP wall is 2.64%. The mean value of the difference between the predicted and monitored displacements of the FP wall is 3.12%. The mean value of the DPMS of FP walls is 3.44%. It shows that the research method can predict the FP data better in practical application. It is more accurate in predicting the changes in displacement and settlement. The research method is used to track the resistance change of the support during construction in order to further test the BC of the support method.

Bearing capacity refers to the maximum capacity that a structure, foundation, or component can bear under a load. That is, the maximum load it can withstand without damage or excessive deformation. In Fig. 9, as the construction process of the subway FP advances, the support method is increased from one layer to three layers. The BC of the overall support structure (SuS) is gradually increased by the support method. When the construction process reaches 11%, one layer of support method is completed, and the BC of the SuS can reach 1176 kPa. When the construction process reaches 20%, the wall support erection is completed, and the BC of the SuS can reach 1913KPa. When the construction process reaches 30%, the second layer of support method is completed, and the BC of the SuS can reach 2687 kPa. When the construction process reaches 42%, the three-layer support method is completed, and the BC of the SuS can reach 3262KPa. It shows that the research model can effectively monitor the mechanical changes during the construction of the support. Moreover, it monitor the BC of the support and the displacement and deformation of the wall in time. To detect the mechanical monitoring effect of the research method, the prediction of the force state of the wall is obtained as shown in Fig. 10.

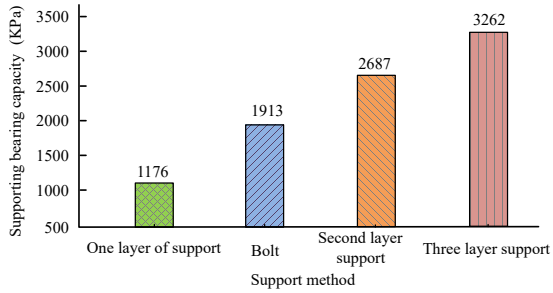

Fig. 9. Monitoring of changes in bearing capacity of support

The monitoring condition's change in the axial force (AF) of the walls on either side of the FP in Fig. 10(a) demonstrates a trend toward lowering as the displacement distance increases. The trend of predicting the AF by LSTM- FLAC method is basically consistent with the monitoring results. The wall AF's average PA is 95.16%. As the displacement distance increases, the shear force of the walls on either side of the FP under the monitoring state displays a decreasing trend. The LSTM-FLAC method's prediction of the AF trend is essentially in line with the monitoring data. 96.43% is the average PA of wall shear force. In Fig. 10(b), the trend of predicting AF by BP method is consistent with the trend of monitoring results, but the average PA of wall AF is only 89.56%. The trend of predicting AF by BP method is also consistent with the trend of monitoring results, but the average PA of wall shear force is 86.11%. It shows that the research method is more accurate in predicting the mechanical state of FP walls, which is 5.6%-10.32% higher compared to the prediction effect of the BP method.

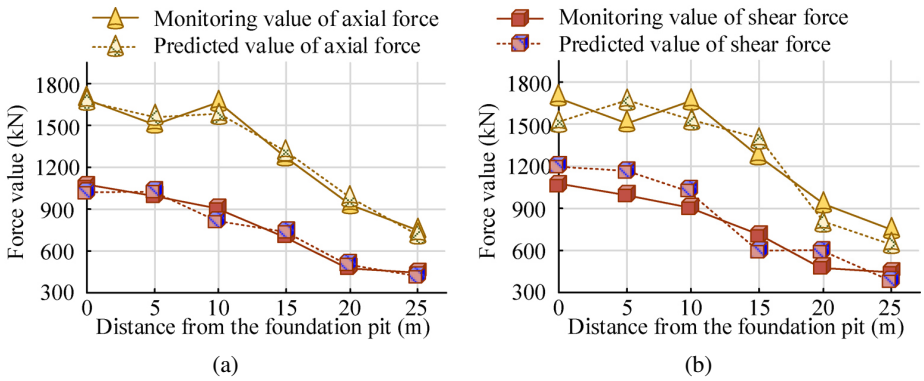

Fig. 10. Monitoring of the stress state of FP: (a) Monitoring effectiveness of LSTM-FLAC method, (b) Monitoring effectiveness of BP method

4. Conclusions

To ensure the safety during the construction of subway FP, the study proposed a data monitoring model based on force prediction. The research method analyzed the offset direction of the SL according to the SL pressure calculation, classified the deformation structure of the SL, and determined the corresponding support measures. Stability analysis was carried out by means of the support method and support level, and the deformation resistance of the support was calculated. The study simulated the displacement change of FP wall with the help of three-dimensional simulation mechanical analysis. Combined with the regularity of monitoring data, it predicted the trend of FP wall changes and the bearing effect of the corresponding support. The outcomes revealed that the CPU utilization of the running machine was 33.17-54.22% when predicting the deformation state of the subway FP with the LSTM-FLAC model. The average segmentation bandwidth of the running machine was 62.17-85.26Mbps when performing the prediction of 50 pieces of data synchronously with the research method. It was also 17.43-45.23% higher than the network bandwidth of the BP network prediction model, which indicated that the research model was more effective. Furthermore, the mechanical state of FP was predicted with the research model. The PA of AF change was shown to be 95.16% and that of shear force change was shown to be 96.43%, which was 5.6-10.32% higher compared to other methods. The research model does not account for the impact of temperature-related changes in SL data, rendering it unsuitable for monitoring data in the context of seasonal temperature fluctuations. Accordingly, subsequent research should include an analysis of the SL state under different temperatures, thereby enhancing the data content of the research model and providing a reliable theoretical model for the data monitoring of subway FPs.

References

[1] Z. Luo, J. Guo, J. Han, and Y. Wang, “Research on the construction safety risk assessment of prefabricated subway stations in China”, *Engineering, Construction and Architectural Management*, vol. 31, no. 4, pp. 1751–1787, 2024, doi: 10.1108/ECAM-04-2022-0340.

[2] S. Amiri and A.N. Dehghan, "Comparison of shallow tunneling method with pile and rib method for construction of subway station in soft ground", *Frontiers of Structural and Civil Engineering*, vol. 16, no. 6, pp. 704–717, 2022, doi: 10.1007/s11709-021-0746-4.

[3] Z. Zhou, Z. Chen, B. Wang, C. Jiang, T. Li, and W. Meng, "Study on the applicability of various in-situ stress inversion methods and their application on sinistral strike-slip faults", *Rock Mechanics and Rock Engineering*, vol. 56, no. 4, pp. 3093–3113, 2023, doi: 10.1007/s00603-022-03199-7.

[4] H. Fan, Y. Liu, Y. Xu, and H. Yang, "Surface subsidence monitoring with an improved distributed scatterer interferometric SAR time series method in a filling mining area", *Geocarto International*, vol. 37, no. 25, pp. 8979–9001, 2022, doi: 10.1080/10106049.2021.2007300.

[5] H. Waqas, M. Hussain, M. Alqarni, M.R. Eid, and T. Muhammad, "Numerical simulation for magnetic dipole in bioconvection flow of Jeffrey nanofluid with swimming motile microorganisms", *Waves in Random and Complex Media*, vol. 34, no. 3, pp. 1958–1975, 2024, doi: 10.1080/17455030.2021.1948634.

[6] Y. Dong, Y. Luan, F. Wang, H. Yang, Z. Jia, and H. Luan, "Monitoring and prediction of horizontal displacement of underground enclosure piles in subway foundation pits", *ACS Omega*, vol. 8, no. 26, pp. 23389–23400, 2023, doi: 10.1021/acsomega.2c00582.

[7] Q. Zhang, Y. Ma, B. Zhang, L. Tian, and G. Zhang, "Time series prediction on settlement of metro tunnels adjacent to deep foundation pit by clustering monitoring data", *KSCE Journal of Civil Engineering*, vol. 27, no. 5, pp. 2180–2190, 2023, doi: 10.1007/s12205-023-0274-y.

[8] M. Wang, D. Zhao, W. Wang, P. Ma, and S. Jiang, "Deformation law and spatial effect of deep foundation pits for subway construction in soil- rock composite strata in seasonally frozen areas", *Tehnički Vjesnik*, vol. 30, no. 4, pp. 1315–1325, 2023, doi: 10.17559/tv-20230208000333.

[9] Y. Liu, F. Huang, G. Wang, Y. Cao, and B. Li, "Study on long- span and variable-section foundation pit excavation in muddy silty clay", *International Journal of Civil Engineering*, vol. 22, no. 5, pp. 739–755, 2024, doi: 10.1007/s40999-023-00905-6.

[10] T. Feng, C. Wang, J. Zhang, K. Zhou, and G. Qiao, "Prediction of stratum deformation during the excavation of a foundation pit in composite formation based on the artificial bee colony-back-propagation model", *Engineering Optimization*, vol. 54, no. 7, pp. 1217–1235, 2022, doi: 10.1080/0305215X.2021.1919100.

[11] H. Sun, E. Gao, and A. Zhou, "Numerical simulation of uneven settlement of municipal solid waste landfill by FLAC 3D", *Waste Management & Research*, vol. 40, no. 4, pp. 374–382, 2022, doi: 10.1177/0734242X211066703.

[12] C. Song, X. Hu, Z. Chen, and W. Huang, "Study on stress-fluid coupling of coal seam floor water outburst based on FLAC 3D simulation", *Chemistry and Technology of Fuels and Oils*, vol. 59, no. 6, pp. 1304-1312, 2024, doi: 10.1007/s10553-024-01648-3.

[13] H. Jing, X. Guo, and P. Yang, "PFC-FLAC coupling-based numerical simulation of triaxial test on soybean granular material", *Particulate Science and Technology*, vol. 42, no. 4, pp. 527–540, 2024, doi: 10.1080/02726351.2023.2267492.

[14] X. Zhang, K. Luo, T. Wang, M. Jiang, J. Feng, and G. Mei, "Microscopic mechanism of coarse-grained soil under triaxial test based on PFC-FLAC coupling method", *Soil Mechanics and Foundation Engineering*, vol. 60, no. 4, pp. 323–329, 2023, doi: 10.1007/s11204-023-09897-w.

[15] P. Miao, H. Yokota, and Y. Zhang, "Deterioration prediction of existing concrete bridges using a LSTM recurrent neural network", *Structure and Infrastructure Engineering*, vol. 19, no. 4, pp. 475-489, 2023, doi: 10.1080/15732479.2021.1951778.

[16] S. Sun, C. Xu, A. Wang, Y. Yang, and M. Su, "Safety evaluation of urban underground utility tunnel with the grey clustering method based on the whole life cycle theory", *Journal of Asian Architecture and Building Engineering*, vol. 21, no. 6, pp. 2532–2544, 2022, doi: 10.1080/13467581.2021.2007104.

[17] C. Heng, S. Sun, J. Zhang, and Z. Zhou, "Calculation method of underground passage excavation on interactive effects among pipe-roof, steel bracing and foundation soil", *KSCE Journal of Civil Engineering*, vol. 26, no. 1, pp. 448-0459, 2022, doi: 10.1007/s12205-021-0500-4.

[18] Z. Li, L. Xu, and X. Deng, "An improved method for slab track- soil interaction considering soil surface deformation", *Mechanics Based Design of Structures and Machines*, vol. 52, no. 7, pp. 42600-4283, 2024, doi: 10.1080/15397734.2023.2225094.

[19] Y. Liu, X. Chen, and M. Hu, "Three-dimensional large deformation modeling of landslides in spatially variable and strain- softening soils subjected to seismic loads", *Canadian Geotechnical Journal*, vol. 60, no. 4, pp. 4260-437, 2022, doi: 10.1139/cgj-2022-0106.

[20] X.M. Long, Y.J. Chen, and J. Zhou, "Development of AR experiment on electric-thermal effect by open framework with simulation- based asset and user-defined input", *Artificial Intelligence and Applications*, vol. 1, no. 1, pp. 52-057, 2023, doi: 10.47852/bonviewAIA2202359.

[21] X. Li, J. Wang, and C. Yang, "Risk prediction in financial management of listed companies based on optimized BP neural network under digital economy", *Neural Computing and Applications*, vol. 35, no. 3, pp. 2045-02058, 2023, doi: 10.1007/s00521-022-07377-0.

[22] Y. Song and J. Cao, "An ARIMA-based study of bibliometric index prediction", *Aslib Journal of Information Management*, vol. 74, no. 1, pp. 94-0109, 2022, doi: 10.1108/AJIM-03-2021-0072.

Received: 2024-10-21, Revised: 2025-04-02